IEEE Access
Multidisciplinary | Rapid Review | Open Access Journal

Received 8 June 2023, accepted 24 June 2023, date of publication 28 June 2023, date of current version 5 July 2023.

Digital Object Identifier 10.1109/ACCESS.2023.3290150

RESEARCH ARTICLE

Running State Monitoring of Induction Motors Based on KPCA_RBF and Stator Current Characteristics

XIAO SONG, YELIN HU, BIN DAI, AND XIAOLIANG ZHENG
School of Safety Science and Engineering, Anhui University of Science and Technology, Huainan 232001, China
Corresponding author: Xiao Song (song-xiao@foxmail.com)

ABSTRACT Induction motors are important equipment in industrial production processes. To solve the problem of characteristic harmonics overlapping when there is deterioration in different parts of the induction motor and diagnose the deterioration degree of internal components such as bearings, stator winding insulation, and air gap balance, a diagnostic method based on kernel principal component analysis (KPCA) and radial basis function neural network (RBF) is proposed. Firstly, through the experimental analysis, it is found that the 2nd, 3rd, 4th, and 5th order characteristic frequency harmonics in the current can reflect the deterioration of the motor. Secondly, KPCA is used to determine the correlation degrees between characteristic frequency harmonic contents and the deterioration of the corresponding parts of the motor. Finally, the products of characteristic frequency harmonic contents and corresponding correlation degrees are taken as the input vectors of radial basis neural network, and the deterioration degrees are taken as the output vectors to diagnose the deterioration of the motor. Through the diagnostic analysis of the experimental unit and the comparison of the actual deterioration degree of the motor after disassembly, it is proved that the proposed method can accurately diagnose the deterioration of the motor. By the proposed method, the correlation between motor deterioration and characteristic frequency harmonics has been identified, and the degree of deterioration of each part of the motor has been quantified. It can monitor the degree of motor deterioration in real-time, grasp the trend of motor deterioration, and detect early signs of motor deterioration.

INDEX TERMS Induction motor, diagnosis, harmonic, kernel principal component, radial basis function neural network.

I. INTRODUCTION

Motors are the largest and most widely used industrial equipment in various production activities of human society. In the industrial field, equipment in factories is basically driven by motors, and motors play an important role in human production and life. However, motors are easily subject to failure during their lifespan due to factors such as bad working environment, load fluctuations, frequent startups, and power grid energy quality. Once a motor fails, it can bring huge losses and seriously affect people's production and life. In order to avoid economic losses and production accidents caused by motor failure, real-time monitoring of motor running state is of great significance. Therefore, how to accurately diagnose the motor fault has become a research hotspot. If the running state of motors can be monitored in real time, motor failures can be predicted early.

Currently, there are mainly three types of methods for motor state monitoring and fault diagnosis. The first type of diagnostic method is based on analytical models. This kind of method has high diagnostic accuracy by establishing an accurate mathematical model for the motor fault diagnosis. It mainly includes: system state estimation method, system state parameter estimation method, and equivalent space method. For example, based on the fractional mathematical model and untracked Kalman filter, the permanent magnet synchronous motor current fault diagnosis model was established [1]. Aiming at the fractional characteristics of

The associate editor coordinating the review of this manuscript and approving it for publication was Qinfen Lu.

This work is licensed under a Creative Commons Attribution-NonCommercial-NoDerivatives 4.0 License.
For more information, see https://creativecommons.org/licenses/by-nc-nd/4.0/

electromagnetic coupling and friction in permanent magnet synchronous motor system, the state space equation of fractional model was established, and a fault detection method with the relative change rate was proposed based on Kalman filter algorithm [2]. In order to effectively detect minor motor faults, a full-dimensional state observer was designed based on the fractional order model to obtain more effective residuals [3]. To detect rotor eccentricity fault, a multi-physical model was proposed to generate vibration displacement of permanent magnet synchronous motor [4]. In order to detect static eccentricity of permanent magnet synchronous motor, the normal and eccentric permanent magnet synchronous motor models based on finite element analysis was established [5]. In order to study the fault-tolerant control strategy, a model of polyphase permanent magnet synchronous motor under phase-out fault was established [6]. In order to diagnose the stator winding inter-turn short circuit fault, a permanent magnet synchronous motor model considering full-space harmonics was established based on winding function [7]. In order to diagnose motor bearing faults, a permanent magnet synchronous motor model considering bearing damage was established [8], [9]. For linear systems, fault diagnosis can be accurately performed through the establishment of analytical models. However, motors are nonlinear systems, and it is difficult to establish an accurate system state model. Therefore, fault diagnosis methods based on analytical models are rarely applied to industrial sites.

The second type of diagnostic method is based on signal processing. This kind of method does not need to establish an accurate mathematical model, but only needs to collect time-domain signals such as current, vibration and sound from the equipment in real time, and then analyze these signals with signal processing technology to obtain equipment state parameters, and monitor these parameters to diagnose equipment faults. For example, the wavelet transform was used to decompose the signal into multiple frequency bands, and then the signals of each frequency band were analyzed and calculated to diagnose the state of the equipment, which could effectively reduce noise interference [10]. The variational mode decomposition method based on cuckoo search algorithm (CSA-VMD) was used to process non-stationary vibration signals, and the optimal scale-morphology slice bispectrum (OSMSB) technology was used to analyze the spectrum, which could enhance the fault characteristics and detect the bearing outer ring faults [11]. Ensemble empirical mode decomposition (EEMD), wavelet threshold (WT) and modulation signal bispectrum (MSB) were used for multistage noise reduction to extract pulse features from the vibration signals, so as to improve the accuracy of motor bearing inner ring and outer ring fault diagnosis [12]. Vibration signals were analyzed using weighted average ensemble empirical mode decomposition (WAEEMD) and modulation signal bispectrum (MSB) to extract characteristic frequencies for bearing fault detection [13]. In order to detect the faults of the bearing and impeller of the centrifugal pump, the characteristics of vibration signals were extracted by modulation signal bispectrum (MSB) [14]. In order to suppress noise interference, second-order total variational denoising (TVD) and modulation signal bispectrum (MSB) were used to process impact signals of rolling bearings, so as to realize effective fault diagnosis of rolling bearings [15]. A method combining the tunable Q-factor wavelet transform (TQWT) and non-dominated negative entropy was proposed to deal with weak transient periodic signals, which could diagnose minor faults of rolling bearings [16]. To detect early faults in rolling bearings, some methods were proposed, such as Minimum entropy deconvolution (MED), detrended wave analysis (DFA) and improved K-nearest neighbor algorithm (IKNN), improved VMD-FRFT based on ICF, feature adaptive method based on candidate fault frequency optimization graph, and method combined with regression strategy, improved variational mode decomposition (VMD) and infographic, and method based on mahalanobis distance and cumulative sum [17], [18], [19], [20], [21].

The third type of diagnostic method is based on knowledge. This kind of method uses learning models to diagnose industrial equipment without establishing accurate system models, it is suitable for fault diagnosis of relatively complex industrial equipment or systems. For example, the residual convolution neural network of multi-scale kernel function was used to process vibration signals to diagnose motor faults [22]. Based on the physical characteristics of vibration signals, a cascade convolutional neural network with progressive optimization was proposed to be suitable for motor fault diagnosis under non-stationary conditions [23]. A two-dimensional multi-scale cascade convolutional neural network was proposed to solve bearing fault diagnosis under different working conditions [24]. In order to avoid the convolutional neural network falling into local optimization, an improved multi-scale cascade convolutional neural network was proposed, which could enhance the input classification information and improve the effectiveness of bearing fault diagnosis [25]. Combined with particle swarm optimization algorithm, adaptive deep convolutional neural network was proposed, which could improve the robustness of bearing fault diagnosis [26]. In order to diagnose the stator winding inter-turn short circuit fault, direct magnetic field orientation control method based on deep neural network, convolutional neural network, convolutional neural network based on wavelet kernel, combined with wavelet transform and back-propagation neural network were proposed [27], [28], [29], [30]. In order to estimate the severity of motor faults, a hierarchical convolutional neural network with feature inheritance was proposed based on stator current signals [31]. The convolutional neural network combined with batch normalization could simultaneously detect the motor bearing fault and rotor broken bar fault [32]. Combining the deep convolutional neural network with the improved Dempster-Shafer theory based on evidence fusion, motor faults could be diagnosed under different load conditions [33]. In terms of bearing fault diagnosis,

deep integrated dense convolutional neural network, deep feature alignment adaptive network, integrated deep neural network and convolutional neural network have also been proposed [34], [35], [36]. Kuncan et al proposed to apply the one-dimensional local binary pattern (1D-LBP) method to vibration signals to improve the accuracy of bearing fault feature extraction [37], [38]. To improve the fault diagnosis accuracy of rolling bearings under varying operating conditions, Zhao et al proposed a method based on joint domain adaptation (JDA) and deep belief networks (DBN) combined with an improved sparrow search algorithm (CWTSSA) [39]. To understand the intrinsic mechanism of deep convolutional neural networks in rolling bearing fault diagnosis, Yang et al proposed to use neuron activation maximization and saliency map methods to visualize the diagnostic knowledge learned by deep neural networks [40]. Bayram et al proposed to use wavelet analysis to obtain the wavelet coefficients of vibration signals and achieve the classification of bearing fault types [41].

In summary, for the single-part faults of motors, such as bearing failures, broken rotor bars failures, and stator inter-turn faults, a large amount of research has been conducted, which can effectively classify the faults and normal states, but cannot determine the degree of deterioration. As the operating time increases, various parts inside the motor will experience deterioration, and the characteristics of deterioration in different parts overlap. It is urgent to find the correlation between the deterioration and characteristics of different parts and accurately determine the degree of deterioration of multiple parts inside the motor.

In order to monitor the degree of deterioration of multiple parts inside the motor in real-time, find the correlation between deterioration and characteristic harmonics, and solve the problem of overlapping features, a motor running state monitoring method based on KPCA_RBF and current characteristics is proposed in this paper. Firstly, the current signal of the motor stator winding is collected. Then, the correlation degree of characteristic harmonics in motor deterioration is obtained by kernel principal component analysis. Finally, the radial basis neural network is used to output the deterioration degree of four parts inside the motor.

II. MOTOR STATE AND HIGHER HARMONICS

Motor is a power device that converts electrical energy into mechanical energy based on electromagnetic theory. It is composed of circuits, magnetic circuits, insulation and mechanical parts. The circuit and magnetic circuit are the main factors that affect the components of the stator current. The formation process and manifestation of abnormal operation states of the motor are diverse, such as insulation aging of the stator winding, bearing wear, and rotor eccentricity, etc., which cause different changes in the current components. If the inherent relationship between the harmonic components of the motor current and the operating status of the motor can be found, the operation condition of the motor can be judged and evaluated. However, it is difficult to describe the relationship between current harmonics and motor operating status by establishing an accurate model. Therefore, it is necessary to use neural networks and a large number of data samples for training to find their inherent rules.

If the stator winding is locally overheated, it will accelerate insulation aging, damage the insulation state, cause changes in the winding impedance, and cause distortion in the magnetic flux waveform, resulting in harmonic flux. Harmonic induced current is produced under the influence of harmonic flux, and the harmonics in the current mainly manifest as odd harmonics. When the center of the stator and the axis of the rotor are not aligned, it will cause uneven air gap and changes in the air gap magnetic field, thereby affecting the magnetic potential and induced electromotive force in the winding, resulting in harmonic current, which is mainly manifested as odd harmonic.

When the internal air gap of the motor is significantly unbalanced due to dust and overheating of the winding, irregular oscillation components appear in the motor current, with the fifth harmonic being enhanced. The reverse torque caused by the fifth harmonic reduces the efficiency of the motor.

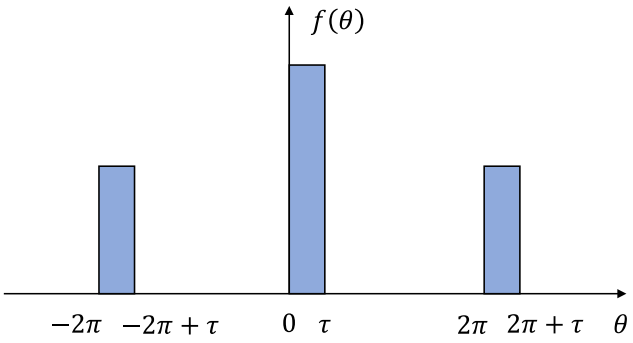

FIGURE 1. Pulse shock wave.

If there is a failure in mechanical parts such as bearings and rotating shafts, it will generate impact pulses as shown in Fig. 1. Where $f(\theta)$ is the function describing the impact pulses. The impact pulses are transmitted to the conductor, causing small movements in the conductor, and even harmonics appear in the eddy currents generated by this movement. An induction motor is composed of a winding section that generates electromagnetic effects and a mechanical section that transmits power, and these two sections influence each other. Therefore, when any abnormal condition occurs in the equipment, both odd and even harmonics will appear in the stator winding current, and the content of various harmonics in the stator winding current will vary depending on the specific abnormal condition.

The motor is the driving system, so its operating state is related to the fundamental wave and the 2nd, 3rd, 4th, and 5th harmonics, which have high energy and low frequency.

The structure of the motor is shown in Fig. 2. The four parts of the motor monitored in this paper are: motor side bearing, stator winding, load side bearing and air gap.

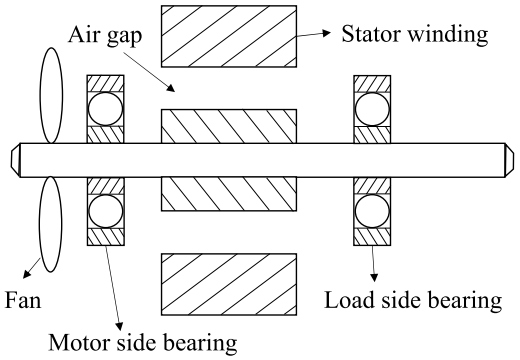

FIGURE 2. Motor cross-sectional diagram.

III. MODEL PRINCIPLE AND ESTABLISMENT

A. PRINCIPLE OF KPCA

Principal Component Analysis (PCA) is an algorithm for linear dimension reduction of data, but when extracting features from data with non-linear relationships, it cannot fully preserve the characteristic information of the data. Kernel Principal Component Analysis (KPCA) combines kernel functions based on PCA, which maps data to a high-dimensional feature space, and then uses linear methods to extract features in the mapped feature space. KPCA can effectively improve the efficiency of feature extraction while fully preserving the characteristic information of the data.

Let x be a dataset with n samples, $x = \{x_1, x_2, \cdots x_n\}$, where $x_i \in R^N$, and each sample has m attributes, then $x_i = \{x_{i1}, x_{i2}, \cdots x_{im}\}$, construct an initial sample matrix $X'_{n\times m}$ based on the input samples, and normalize it to obtain a sample matrix $X_{n\times m}$ [42].

First, the samples are mapped to the high-dimensional feature space R^F by a mapping function φ, the corresponding mapped values are $\varphi(x_1), \varphi(x_2), \cdots, \varphi(x_n)$, and then using PCA method to solve, the covariance matrix C can be written as:

$$C = \frac{1}{n}\sum_{i=1}^{n} \varphi(x_i)\,\varphi(x_i)^T \tag{1}$$

Its characteristic equation is as follows:

$$Cv = \lambda v \tag{2}$$

where λ is the eigenvalue of the covariance matrix and $v$is the eigenvector, and it can be solved from equations (1) and (2):

$$v = \sum_{i=1}^{n} \varphi(x_i)\frac{\varphi(x_i)^T v}{\lambda n} = \sum_{i=1}^{n} \varphi(x_i)\alpha_i \tag{3}$$

where $\alpha_i = \frac{\varphi(x_i)^T v}{\lambda n}$. Usually, the mapping function φ is not explicit and the calculation of v can be difficult. Therefore, a kernel function is introduced as follows:

$$k(x_i, x_j) = \phi(x_i)^T \phi(x_j) \tag{4}$$

For equation (2), any $k = 1, 2, \cdots, n$ has:

$$\varphi(x_k)\,Cv = \lambda\varphi(x_k)\,v \tag{5}$$

Substituting equations (1), (3), and (4) into equation (5), we get:

$$K\alpha = \lambda n\alpha \tag{6}$$

where K is the kernel matrix corresponding to k, and it is defined as: $K = k(x_i, x_j)$, $\alpha = (\alpha_1, \alpha_2, \cdots, \alpha_n)$.

Through Equation (6), the eigenvalues $\lambda_1 \geq \lambda_2 \geq \cdots \lambda_n$ and their corresponding eigenvalues $\alpha_1, \alpha_2, \cdots, \alpha_n$ can be obtained. Select p $(p \leq n)$ eigenvalues to meet the cumulative contribution rate $\geq$ 85%. The j-th $(j = 1, 2, \cdots, p)$ coordinate of the new projected sample $\varphi(x_j)$ is given by:

$$y_j = \sum_{i=1}^{n} \alpha_i^j \left(\varphi(x_i)^T \varphi(x_j)\right) = \sum_{i=1}^{n} \alpha_i^j k(x_i, x_j) \tag{7}$$

where α_i has already been normalized, and α_i^j is the j-th component of α_i. Normalization should meet the following requirements:

$$\alpha_i^T \alpha_i = \frac{1}{\lambda_i} \tag{8}$$

B. KERNEL FUNCTION SELECTION

Kernel functions are classified into local kernel functions and global kernel functions, and the selection of kernel functions often affects the effectiveness of KPCA data dimensionality reduction. To better preserve the feature information of the data, this paper combines two types of kernel functions with weighted combination to build a new kernel function. The kernel function parameters are obtained by multiple experiments, and the proportion coefficients of the combined kernel function are selected using grid search to achieve the maximum contribution rate. Kernel functions used are Gaussian kernel function (local kernel function) and polynomial kernel function (global kernel function) [42]:

$$k(x, x') = exp\left(-\frac{\|x - x'\|^2}{2\sigma^2}\right) \tag{9}$$

$$k(x, x') = (\gamma(x, x') + a)^d \tag{10}$$

where σ is the undetermined parameter of Gaussian kernel function, while γ, a and d are the undetermined parameters of polynomial kernel function.

By weighted combination of Equation (9) and Equation (10), we can get:

$$k(x, x') = \eta_1 \times exp\left(-\frac{\|x - x'\|^2}{2\sigma^2}\right) + \eta_2 \times (\gamma(x, x') + a)^d \tag{11}$$

where η_1 and η_2 are the proportional coefficients of the combined kernel function.

C. PRINCIPLE OF RBF

Like BP neural network, radial basis network belongs to nonlinear multilayer forward network, which can be divided into two models: regularization network and generalized network. In this paper, generalized network is selected. The RBF network usually consists of three layers, namely input layer, hidden layer and output layer. The number of neurons in the input layer is equal to the number of attributes of the sample data, while the number of neurons in the hidden layer of the regularization network is equal to the total number of sample data. In generalized networks, the number of neurons in the hidden layer is generally between the number of attributes in the sample data and the total number of sample data. The activation function of the hidden layer is the radial basis function, and generally, the Gaussian function is selected as the activation function. The activation function of the output layer is a linear function. Its network structure is shown in Fig. 3, where the activation function of the node of the hidden layer uses radial basis function to process the input variables, and then maps linearly to the output layer [43].

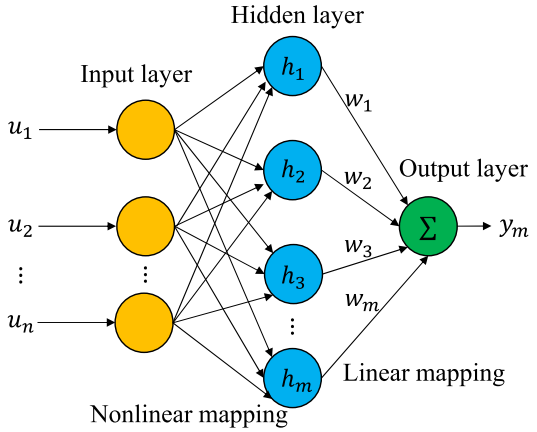

FIGURE 3. Stucture of RBF.

In the RBF network structure, $U = [u_1, u_2, \cdots, u_n]^T$ is an n-dimensional input variable, and the radial basis vector of the hidden layer can be expressed as:

$$H = [h_1, h_2, \cdots, h_m]^T \tag{12}$$

where m is the number of nodes in the hidden layer and h is the Gaussian radial basis function, then h_m can be expressed as [43]:

$$h_m = exp\left(-\frac{\|U - c_m\|^2}{2b_m^2}\right) \tag{13}$$

In the equation, $C = [c_1, c_2, \cdots, c_m]^T$ is the central parameter of the hidden layer nodes, $B = [b_1, b_2, \cdots, b_m]^T$ is the width parameter of the radial basis function, $W = [w_1, w_2, \cdots, w_m]^T$ is the network weight parameter from the hidden layer to the output layer, then the output of the RBF network at moment k can be expressed as [43]:

$$y(k) = \sum_{j=1}^{m} h_j w_j \tag{14}$$

D. KPCA_RBF MODEL CONSTRUCTION

Through the previous analysis, it is known that the degradation level of the bearings, stator winding insulation, rotating shaft and air gap inside the motor is directly related to the 2^{nd} to 5^{th} harmonic contents in the motor current. However, through the experiment, it is found that the correlation between the deterioration of different parts and the 2^{nd} to 5^{th} harmonic contents is different. For example, the correlation between the deterioration of the motor-side bearing and the 2^{nd} harmonic content in the current is relatively high. The insulation deterioration of the stator winding is highly correlated with the 3^{rd} harmonic content in the current, the load-side bearing deterioration is highly correlated with the 4^{th} harmonic content of the current, and the air gap equilibrium deterioration is highly correlated with the 5^{th} harmonic content in the current. Therefore, KPCA was used to determine the correlation degrees of the 2^{nd} to 5^{th} harmonic contents in the deterioration of different parts of the motor, and the products of the 2^{nd} to 5^{th} harmonic contents and their correlation degrees were taken as the input vectors of RBF, and the deterioration degrees of each part of the motor were taken as the output vectors. So, the degradation status of various parts of the motor is being monitored in real-time.

The process of model establishment in this paper is as follows:

Step 1: KPCA was used to process the motor current data and determine the correlation degrees of the 2^{nd} to 5^{th} characteristic harmonics in the deterioration of the corresponding parts of the motor. The specific steps of KPCA are as follows:

(a) Standardize the initial harmonic data of the motor current (standard deviation normalization method is adopted in this paper) and calculate the kernel matrix K.

(b) Since the motor current harmonic data is non-centralized, it needs to be centralized. The centralized kernel matrix is expressed as follows:

$$K^* = K - \frac{1}{n}zz'K - \frac{1}{n}Kzz' + \frac{1}{n^2}\left(z'Kz\right)zz' \tag{15}$$

where z is an n-dimensional vector with all elements equal to 1.

∈ Calculate the eigenvector V and eigenvalue λ of the matrix K^*.

(d) Normalize the eigenvector.

∈ Calculate the cumulative contribution rate $G_1, G_2, \cdots, G_n$ of eigenvalues $\lambda_1, \lambda_2, \cdots, \lambda_n$, and verify whether the contribution rate of the first principal component is consistent with the set cumulative contribution rate p.

(f) According to the factor loading coefficients and eigenvalue λ_1 of the first principal component, calculate the correlation degree of each factor, that is, determine the

correlation degrees $\rho_1, \rho_2, \cdots, \rho_4$ of the 2nd to 5th harmonic contents in the motor deterioration;

(g) Multiply the original sample X with the corresponding correlation degrees $\rho_1, \rho_2, \cdots, \rho_4$ to get the input vectors of the RBF network.

Step 2: Split the original data into training and testing samples.

Step 3: Train the RBF network with training samples.

Step 4: Input test samples into the trained model for independent sample test.

IV. EXPERIMENTAL ANALYSIS AND VERIFICATION

A. EXPERIMENTAL SETUP

In order to obtain the harmonic data of the motor, an experimental setup is constructed as shown in Fig. 4(a). The device is composed of a motor and an AC generator, which are directly connected by a coupling. The parameters of the motor are: insulation class B, rated voltage of 380 V, rated power of 3 kW, rated current of 6.8 A, rated speed of 1500 r/min, efficiency of 82.5%. The generator parameters are: rated power of 2 kW, rated voltage of 400 V, rated current of 3.6 A, excitation voltage of 70 V, excitation current of 3 A, rated speed of 1500 r/min, and insulation Class B.

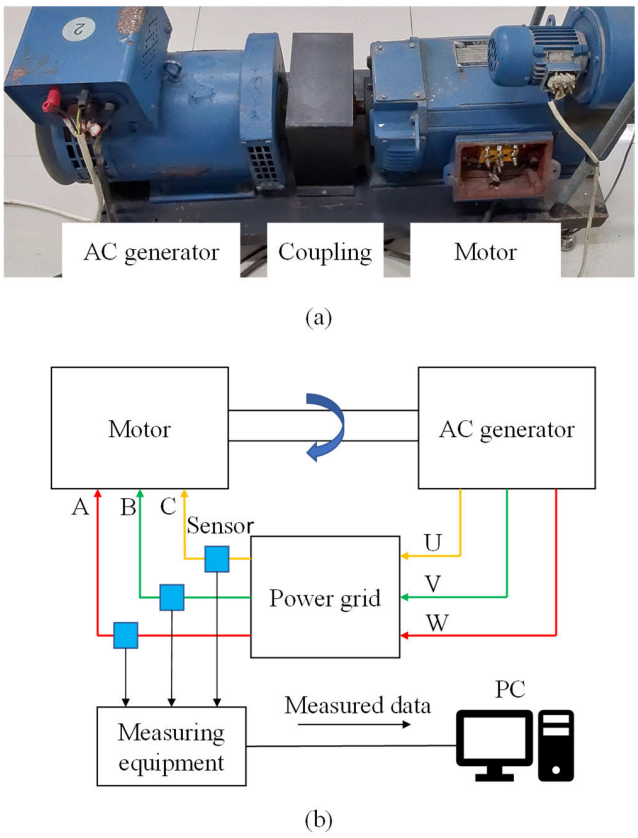

FIGURE 4. Experimental setup. (a) Motor-generator unit. (b) Structure of experimental device.

The structure of the experimental device is shown in Fig. 4(b), including the motor-generator unit and the measurement system. The operation mode of the unit is as follows: the three-phase power of the grid is supplied to the motor, and the motor drives the generator. After the generator is connected to the grid, the electric energy emitted will be returned to the grid. By setting the output power of the generator, the load rate of the motor can be easily controlled. The measuring system collects the current signals through the sensors and uploads them to the upper computer.

In order to obtain the harmonic data in the motor current, the sensor as shown in Fig. 5(a) was designed. This sensor detects the motor current signal through electromagnetic induction, without any electrical connection to the motor power cable. It is easy to install, and only needs to be tied to the three-phase power cable of the motor. Installation can be done without stopping the motor, and real-time motor current signals can be collected without affecting the normal operation of the motor. Its specific parameters are: inductance of 30 mH, DC resistance of 155 Ω.

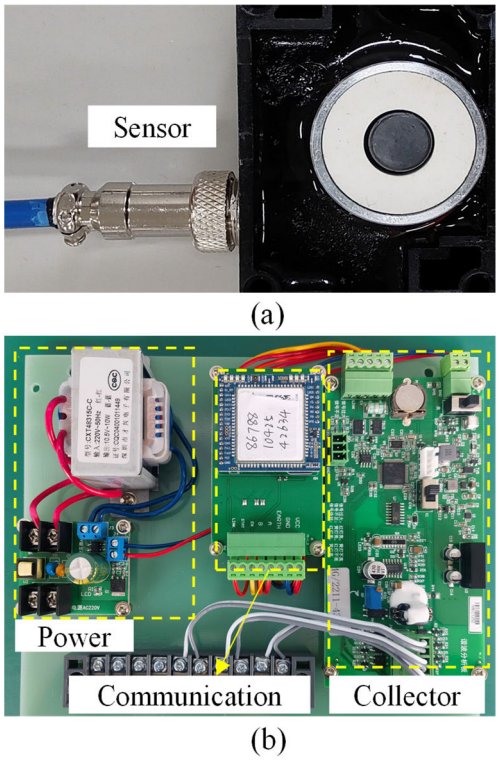

FIGURE 5. Measuring system. (a) The sensor. (b) Measuring equipment.

The designed signal acquisition device is shown in Fig. 5(b). The signal acquisition device is composed of three parts: power supply, data acquisition board and communication board. The power supply part is used to convert single-phase AC power into 12 V DC power to supply power to the data acquisition board and communication board. The data acquisition board is mainly composed of signal auto-gain amplifying and filtering circuit and single-chip microcontroller circuit. The amplifying and filtering circuit is responsible for amplifying and filtering the small signals detected by the sensors. To ensure the accuracy of the

data, it must be able to effectively filter out interference signals, and finally the processed analog signals are sent to the single-chip microcontroller circuit to be converted into digital signals. The single-chip microcontroller circuit is also responsible for performing fast Fourier transform on the collected current data to obtain the harmonic content in the motor current. The communication board is responsible for transmitting the harmonic content data through the 4G network to the upper computer system.

B. EXPERIMENTAL DATASET CONSTRUCTION

To ensure that the collected data can accurately reflect the deterioration of various parts of the motor, the load rate of the motor needs to be above 30%, and the load rate of the motor is set to 60% in the experiment. In the experiment, various deterioration degrees of motor side bearing, load side bearing, stator windings and internal air gap are designed and achieved by replacing parts. The deterioration degrees of various parts are quantified between 0-100%, and the deterioration degrees are divided into four types. The deterioration degrees between 0 and 40% are considered as good, between 41% and 60% as mild deterioration, between 61% and 80% as moderate deterioration, and above 80% as severe deterioration. In the experiment, 8000 data points are collected for each part, with each of the four deterioration degrees having 2000 data points. A total of 32000 data points are collected from the four parts. The dataset is divided into training and testing sets in a ratio of 80% and 20%.

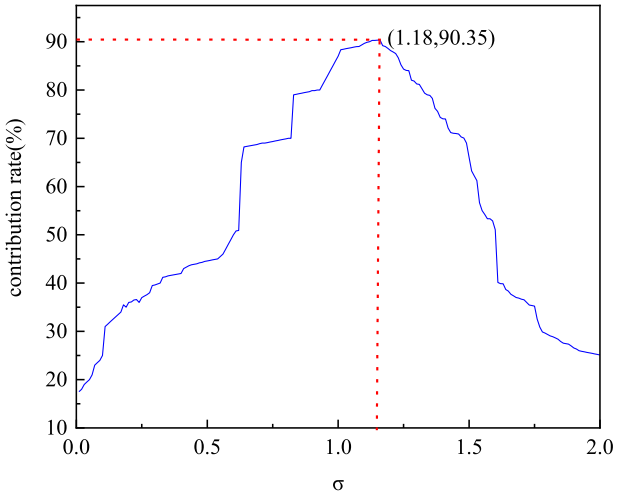

FIGURE 6. The parameter of the gaussian kernel function.

C. MODEL TRAINING RESULTS

In this paper, the collected harmonic data are firstly analyzed by KPCA. In determining the parameter σ of the Gaussian kernel function, a grid search method is used. That is, σ is gradually increased from small to large, and the contribution rate of the first principal component is calculated. The value of σ that maximizes the contribution rate of the first principal component is selected as the parameter of the Gaussian kernel function. The results are shown in Figure 6. As can be seen from the figure, σ is taken as 1.18.

Using the same grid search method, with the maximization of the first principal component as the objective, the parameters of the polynomial kernel function are determined as $a = 1$, $d = 3$, and the combination coefficients are $\eta_1 = 0.8$ and $\eta_2 = 0.2$. The results of KPCA analysis are shown in Table 1.

TABLE 1. The second to fifth harmonic correlation.

Motor parts	Second harmonic correlation	Third harmonic correlation	Fourth harmonic correlation	Fifth harmonic correlation
Motor side bearing	0.55	0.09	0.16	0.06
Stator winding insulation	0.07	0.61	0.05	0.22
Load side bearing	0.23	0.10	0.41	0.08
Air gap balance	0.06	0.20	0.08	0.59

From Table 1, it can be seen that the deterioration of the motor-side bearing is highly correlated with the second harmonic content of the motor current, with a correlation coefficient of 0.55. This indicates that when the motor-side bearing deteriorates, the second harmonic content in the motor current will significantly increase. The insulation deterioration of the stator winding is most highly correlated with the third harmonic content of the current, with a correlation coefficient of 0.61. This indicates that when the third harmonic content of the motor current increases, the insulation of the stator winding has deteriorated. In addition, the insulation deterioration of the stator winding is also highly correlated with the fifth harmonic content of the current, with a correlation coefficient of 0.22. The deterioration of the load-side bearing is most highly correlated with the fourth harmonic content of the current, with a correlation coefficient of 0.41. In addition, it is also correlated with the second harmonic content of the current, with a correlation coefficient of 0.23. The balance of the internal air gap of the motor is highly correlated with the fifth harmonic content of the current, with a correlation coefficient of 0.59. This indicates that when the motor air gap is unbalanced, the fifth harmonic content in the motor current will significantly increase.

The input vectors of the RBF network were obtained by multiplying the contents of the second to fifth harmonics with the corresponding correlation, and the deterioration degrees of each part of the motor were taken as the output vectors to set up the training samples. Input training samples into the RBF network to train the network. The input layer of the RBF neural network has 4 nodes, and the input is a vector of 1 row and 4 columns. The output layer has 1 node. The Mean Squared Error (MSE) goal was set to 0.001, and the radial basis function expansion rate was set to 1.6. The faster the expansion rate, the smoother the training curve will be. There is no need to set a hidden layer in the middle. Instead, the

TABLE 2. Diagnostic accuracy of motor deterioration.

Motor parts	Motor side bearing	Stator winding insulation	Load side bearing	Air gap balance
Diagnostic accuracy (%)	91.30	89.25	92.39	90.70

number of hidden layers can be increased continuously until the output error is satisfied.

The test sample data were input into the trained RBF neural network for testing, and the test results are shown in Table 2. The accuracy of RBF neural network in diagnosing the deterioration of each part of the motor can reach more than 89%.

D. EXAMPLE VERIFICATION 1

In order to verify the accuracy of the model, data were collected in real-time on the unit platform and uploaded to the upper computer through a 4G wireless module. The trained model was then used for diagnosis on the upper computer. Figure 7 shows the original signals collected by the sensor, where Figure 7(a) is the signal when the motor side bearing is deteriorated, and Figure 7(b) is the signal after the motor side bearing is repaired. As can be seen from the figure, the amplitude of the signal is only a little over 2 mV, and it is coupled with a lot of noise signals. Therefore, before analyzing the signal, amplification and filtering must be performed.

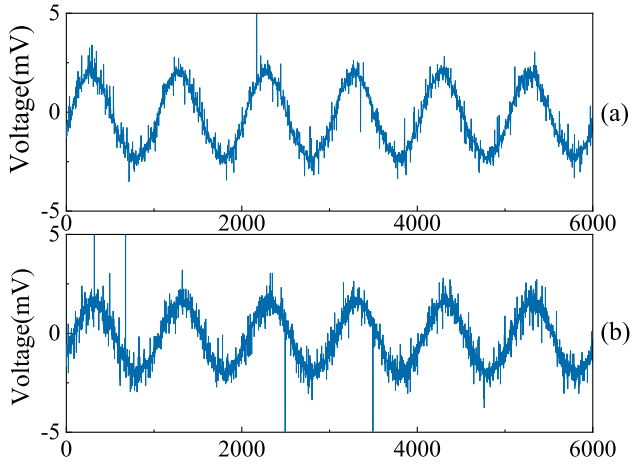

FIGURE 7. Sensor signal. (a) Before maintenance. (b) After maintenance.

The harmonic contents in the motor current at the 9th minute before motor maintenance is shown in Fig. 8(a). It can be seen from the figure that the content of the 2nd harmonic is significantly increased, reaching 2.8%. It can be preliminarily judged that the motor side bearing is deteriorating. However, it is not enough to judge the deterioration of the motor side bearing based solely on the increase in the 2nd harmonic content. This is because poor motor dynamic balance and poor installation can also cause an increase in the content of the 2nd harmonic. Therefore, it is necessary to make a comprehensive judgment by combining the content of other harmonics.

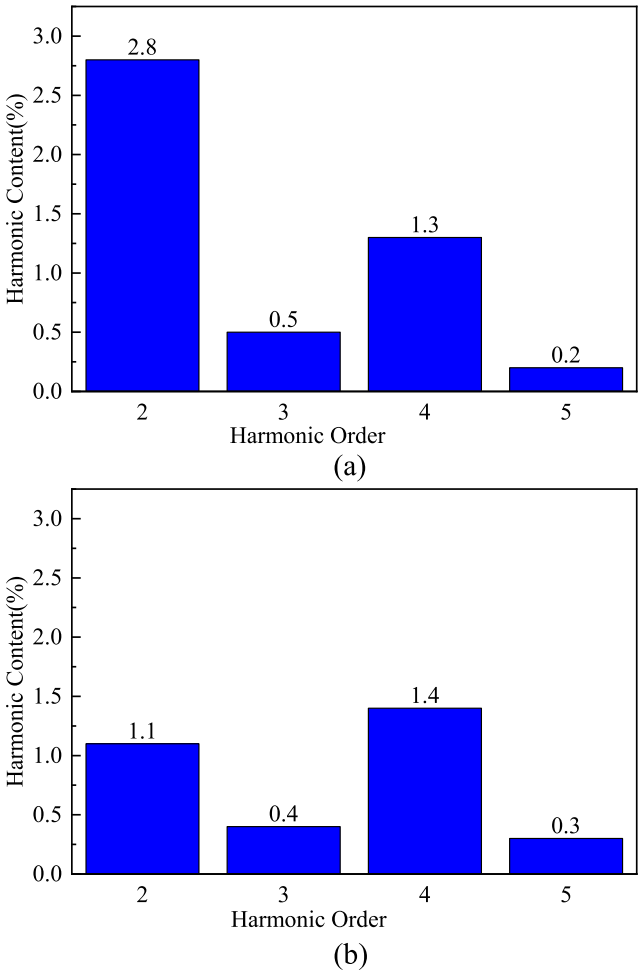

FIGURE 8. Harmonic content. (a) Before maintenance. (b) After maintenance.

The deterioration values of the four parts of the motor at each moment output by the upper computer model are shown in Figure 9, with a sampling and analysis period of one minute. From the pre-maintenance stage in the figure, it can be seen that the deterioration value of the motor side bearing is around 67%, which belongs to moderate deterioration. The deterioration value of the stator winding insulation is around 40%, which is in good condition. The deterioration value of the load side bearing is around 50%, which is a mild deterioration. The deterioration value of the air gap balance is around 38%, which is in good condition. In order to verify whether there is deterioration in the motor side bearing, the motor side bearing was dismantled and observed. As shown in Fig. 10(a), it was found that the bearing was short of oil and had indeed deteriorated. When the bearing operates in a low oil state, it will experience wear, which further exacerbates deterioration. At the same time, it will intensify the vibration of the motor. Bearing oil must be added as soon as possible.

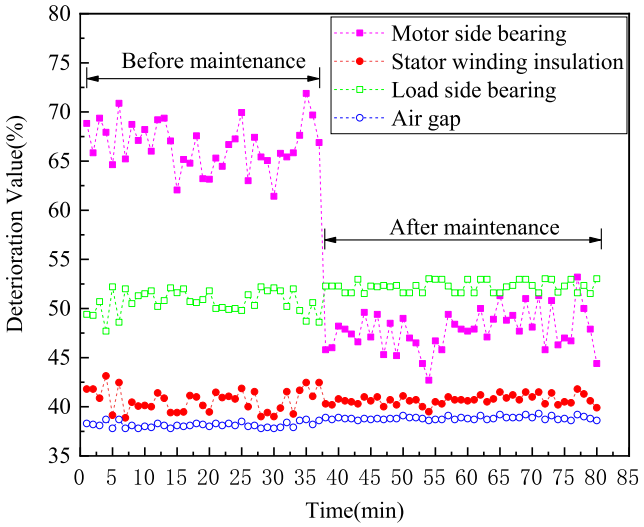

FIGURE 9. Deterioration values of four parts of the motor.

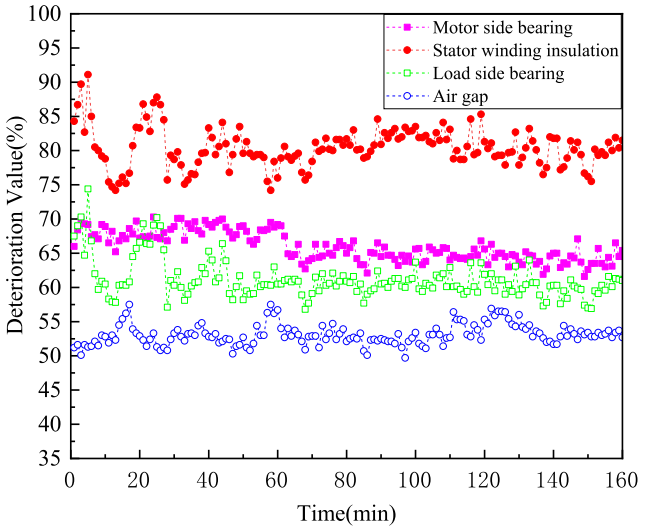

FIGURE 11. Deterioration values of four parts of the motor.

The motor side bearing was repaired and bearing oil was added. The post-repair condition is shown in Fig. 10(b). The harmonic data of the motor after maintenance were collected, and the harmonic content at the 51st minute is shown in Fig. 8(b). As can be seen from the figure, the content of the 2nd harmonic is significantly reduced, dropping to 1.1%. After bearing lubrication, the rotor runs smoothly, the impact on the motor is weakened. The vibration during motor operation is significantly weakened, and the characteristic harmonic contents in the motor current are also significantly reduced. The collected harmonic data were analyzed by the diagnostic model of the upper computer, and the results are shown in Figure 9 after maintenance. It can be seen from the figure that the deterioration value of the motor side bearing has been reduced to about 47%.

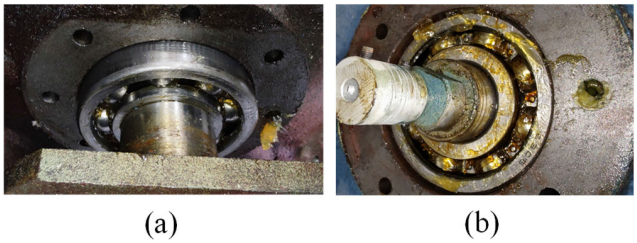

FIGURE 10. Motor bearing state. (a) Before maintenance. (b) After maintenance.

E. EXAMPLE VERIFICATION 2

To verify the effectiveness of the proposed method in industrial field, the developed system was installed on a three-phase asynchronous motor in a paper mill. The parameters of the motor are as follows: rated voltage of 380 V, rated power of 18.5 kW, and rated speed of 500 r/min.

The deterioration levels of the four parts of the motor detected are shown in Figure 11. It can be seen from the figure that many of the deterioration data of the motor stator winding insulation are above 80%, indicating that the stator winding insulation is in a severe deterioration state and must be shut down for maintenance, otherwise the motor is likely to burn out. After disassembly, the stator winding is shown in Figure 12. It can be seen from the figure that the insulation paint on the winding has aged and peeled off, which is consistent with the results we monitored.

It can also be seen from Figure 11 that the deterioration levels of the motor-side bearing and the load-side bearing are between 60% and 70%, and the deterioration level of the motor-side bearing is higher than that of the load-side bearing, which is in a moderate deterioration state. This is mainly due to the long running time of the motor, and the internal bearings will naturally wear and age, which is a normal phenomenon, but the deterioration trend needs to be monitored. The air gap balance between the stator and rotor is in a slightly deteriorated state, with a level between 50% and 60%.

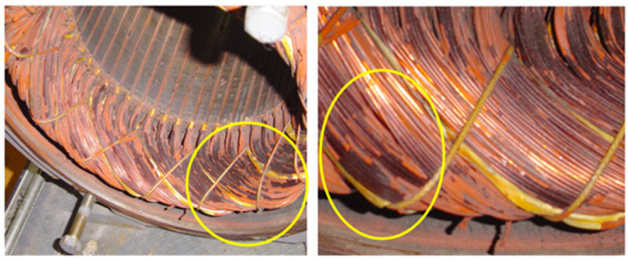

FIGURE 12. Stator winding insulation status.

F. COMPARATIVE RESULTS WITH LITERATURE

From Table 3, it can be seen that many studies focus on a specific type of fault inside the motor, such as stator interturn faults, broken rotor bars, or bearing faults. This paper

TABLE 3. Comparison with results from the literature.

Author(s)	Method	Acquired signals	Fault Type	Accuracy
Skowron et al., 2020	Convolutional neural network (CNN)	Current vector components Voltage vector components	Stator inter-turn (SIT) faults	98%
Ray et al., 2020	Wavelet kernel-based convolutional neural network (WK-CNN)	Stator Current signals	Stator inter-turn (SIT) faults	96.13%
Skowron et al., 2020	Convolutional neural network (CNN)	Stator Current signals	Stator inter-turn (SIT) faults	98.8%
Kumar et al., 2021	Convolutional neural network with batch normalization (CNN-BN)	Vibration signals	Bearing faults Broken rotor bars faults	99.50%
Chan et al., 2021	Feature inherited hierarchical convolutional neural network (FI-HCNN)	Stator Current signals	Eccentricity Broken rotor bars faults Unbalanced conditions	(99.70±0.11%)
Wu et al., 2021	Deep ensemble dense convolutional neural network (DEDCNN)	Vibration signals	Bearing faults	Above 95.06%
Liu et al., 2022	Deep feature alignment adaptation network (DFAAN)	Vibration signals	Bearing faults	(99.32±0.21)%
Li et al., 2019	Ensemble convolutional neural network and deep neural network (CNNEPDNN)	Vibration signals	Bearing faults	95.76%
Kaya et al., 2021	One dimensional gray level co-occurrence matrices	Vibration signals	Bearing faults	Above 87.50%
Kuncan et al., 2020	One-dimensional local binary pattern (1D-LBP) and gray relational analysis (GRA)	Vibration signals	Bearing faults	Above 94.224%
Authors of this article	Kernel principal component analysis (KPCA) and radial basis function neural network (RBF)	Stator Current signals	Motor-side bearing faults Stator winding insulation Load-side bearing faults Air gap	Above 89.25%

focuses on the study of faults in four specific parts inside the motor. Compared with the study of faults in a single part, it is more prone to the problem of feature overlap, which increases the difficulty in the identification rate and accuracy of fault diagnosis. Although the accuracy of the method proposed in this paper for diagnosing faults in a single part may not be as good as other literature, this paper considers the deterioration diagnosis of all four parts inside the motor, and the overall diagnostic accuracy is above 89%, which meets the requirements of industrial field application. In addition, it can provide specific levels of deterioration. It is able to grasp the trend of motor deterioration.

As can be seen from Table 3, the signals collected in the study of motor faults mainly include stator current and vibration signals, both of which contain information about motor faults. The signals collected in this paper are stator current signals, and the designed sensor is easy to install on the industrial site without stopping the motor.

V. CONCLUSION

This paper proposes a motor deterioration diagnosis method based on stator current characteristics. The Kernel Principal Component Analysis (KPCA) is used to determine the correlation between the 2nd to 5th harmonics and the deterioration of various parts of the motor, and the Radial Basis Function (RBF) neural network is used to output the degradation values. This method has found the correlation between motor deterioration and characteristic harmonics, solved the problem of feature overlap, and can perform real-time online monitoring of four parts of the motor, enabling grasp of the trend of motor deterioration, facilitating intervention in the early stage of motor degradation to prevent serious damage

and failure of the motor. The designed sensor and measuring device are easy to install on-site and can be installed without stopping the machine.

Through case analysis, it was found from the degradation chart that the deterioration value of the motor side bearing increased. After disassembling, it was found that the bearing did indeed have a situation of oil shortage and wear. After repairing the motor bearing and adding lubricating oil, the degradation value of the motor bearing in the degradation chart decreased, which proved the effectiveness and real-time performance of this method. It can effectively detect problems with motors in industrial applications.

In this study, only the deterioration of the motor part was monitored in real-time. In the future, research needs to be carried out on the deterioration of the load part, such as the coupling, gear, transmission belt, and rotary shaft. Additionally, the impact of motor load on the deterioration value should also be studied. In terms of diagnostic accuracy, the overall accuracy rate is over 89%, which meets the requirements of industrial applications. However, in the future, other deep learning algorithms can be tried to further improve the diagnostic accuracy.

REFERENCES

[1] W. Yu, C. Wen, and Y. Chen, "Minor fault diagnosis based on fractional-order model of permanent magnet synchronous motor," in *Proc. 43rd Annu. Conf. IEEE Ind. Electron. Soc. (IECON)*, Beijing, China, Oct. 2017, pp. 8082–8086.

[2] W. Yu and C. Wen, "Minor fault detection for permanent magnet synchronous motor based on fractional order model and relative rate of change," in *Proc. Int. Conf. Control, Autom. Inf. Sci. (ICCAIS)*, Oct. 2018, pp. 337–342.

[3] Z. Wang, W. Yu, W. Yu, and C. Wen, "Observer design based on fractional-order model of permanent magnet synchronous motor," in *Proc. IEEE 10th Data Driven Control Learn. Syst. Conf. (DDCLS)*, May 2021, pp. 1257–1262.

[4] K. Alameh, N. Cité, G. Hoblos, and G. Barakat, "Multiphysical modeling for fault detection in permanent magnet synchronous motors," in *Proc. IEEE Int. Conf. Ind. Technol. (ICIT)*, Mar. 2015, pp. 781–786.

[5] R. Abdelli, A. Bouzida, O. Touhami, and M. Ouadah, "Static eccentricity fault modeling in permanent-magnet synchronous motors," in *Proc. 8th Int. Conf. Model., Identificat. Control (ICMIC)*, Nov. 2016, pp. 364–368.

[6] M. Fei and R. Zanasi, "Modeling of multi open phase fault condition of multi-phase permanent magnet synchronous motors," in *Proc. Int. Aegean Conf. Electr. Mach. Power Electron. Electromotion, Joint Conf.*, Sep. 2011, pp. 368–373.

[7] Z. Gherabi, D. Toumi, N. Benouzza, and N. Henini, "Modeling and diagnosis of stator winding faults in PMSM using motor current signature analysis," in *Proc. Int. Aegean Conf. Electr. Mach. Power Electron. (ACEMP) Int. Conf. Optim. Electr. Electron. Equip. (OPTIM)*, Aug. 2019, pp. 227–232.

[8] A. Rezig, A. N'Diaye, M. R. Mekideche, and A. Djerdir, "Modelling and detection of bearing faults in permanent magnet synchronous motors," in *Proc. XX Int. Conf. Electr. Mach.*, 2012, pp. 1778–1782.

[9] C. P. Mbo'o and K. Hameyer, "Modeling of a permanent-magnet excited synchronous machine with bearing damage," in *Proc. 40th Annu. Conf. IEEE Ind. Electron. Soc. (IECON)*, Oct. 2014, pp. 3855–3860.

[10] X. Xu, F. Xiao, and S. Wang, "Enhanced chiller sensor fault detection, diagnosis and estimation using wavelet analysis and principal component analysis methods," *Appl. Thermal Eng.*, vol. 28, nos. 2–3, pp. 226–237, Feb. 2008.

[11] X. Yan and M. Jia, "Application of CSA-VMD and optimal scale morphological slice bispectrum in enhancing outer race fault detection of rolling element bearings," *Mech. Syst. Signal Process.*, vol. 122, pp. 56–86, May 2019.

[12] J. Guo, D. Zhen, H. Li, Z. Shi, F. Gu, and A. D. Ball, "Fault feature extraction for rolling element bearing diagnosis based on a multi-stage noise reduction method," *Measurement*, vol. 139, pp. 226–235, Jun. 2019.

[13] D. Zhen, J. Guo, Y. Xu, H. Zhang, and F. Gu, "A novel fault detection method for rolling bearings based on non-stationary vibration signature analysis," *Sensors*, vol. 19, no. 18, p. 3994, Sep. 2019.

[14] O. Hamomd, S. Alabied, Y. Xu, A. Daraz, F. Gu, and A. Ball, "Vibration based centrifugal pump fault diagnosis based on modulation signal bispectrum analysis," in *Proc. 23rd Int. Conf. Autom. Comput. (ICAC)*, Sep. 2017, pp. 1–5.

[15] D. Zhu, Y. Zhang, L. Zhao, and Q. Zhu, "Fault feature extraction of rolling element bearings based on TVD and MSB," *J. Vib. Shock*, vol. 38, no. 8, pp. 103–109, Aug. 2019.

[16] X. Gu, S. Yang, Y. Liu, Z. Liu, and R. Hao, "Weak fault feature extraction of rolling element bearings based on ensemble tunable *Q*-factor wavelet transform and non-dominated negentropy," *Meas. Sci. Technol.*, vol. 33, no. 6, pp. 1–23, Mar. 2022.

[17] S. Zhao, Q. Song, M. Wang, X. Huang, D. Cao, and Q. Zhang, "An early fault diagnosis method of rolling element bearings based on MED, DFA, and improved KNN," in *Proc. IEEE 3rd Int. Conf. Electron. Inf. Commun. Technol. (ICEICT)*, Nov. 2020, pp. 123–128.

[18] G. Chen, C. Yan, J. Meng, H. Wang, and L. Wu, "Improved VMD-FRFT based on initial center frequency for early fault diagnosis of rolling element bearing," *Meas. Sci. Technol.*, vol. 32, no. 11, Aug. 2021, Art. no. 115024.

[19] A. Babiker, C. Yan, Q. Li, J. Meng, and L. Wu, "Initial fault time estimation of rolling element bearing by backtracking strategy, improved VMD and infogram," *J. Mech. Sci. Technol.*, vol. 35, no. 2, pp. 425–437, Feb. 2021.

[20] Y. Cheng, S. Wang, B. Chen, G. Mei, W. Zhang, H. Peng, and G. Tian, "An improved envelope spectrum via candidate fault frequency optimization-gram for bearing fault diagnosis," *J. Sound Vib.*, vol. 523, pp. 425–437, Apr. 2022.

[21] Q. Li, C. Yan, W. Wang, A. Babiker, and L. Wu, "Health indicator construction based on MD-CUMSUM with multi-domain features selection for rolling element bearing fault diagnosis," *IEEE Access*, vol. 7, pp. 138528–138540, 2019.

[22] R. Liu, F. Wang, B. Yang, and S. J. Qin, "Multiscale kernel based residual convolutional neural network for motor fault diagnosis under nonstationary conditions," *IEEE Trans. Ind. Informat.*, vol. 16, no. 6, pp. 3797–3806, Jun. 2020.

[23] F. Wang, R. Liu, Q. Hu, and X. Chen, "Cascade convolutional neural network with progressive optimization for motor fault diagnosis under nonstationary conditions," *IEEE Trans. Ind. Informat.*, vol. 17, no. 4, pp. 2511–2521, Apr. 2021.

[24] L. Zhang, Y. Lv, W. Huang, and C. Yi, "Bearing fault diagnosis under various operation conditions using synchrosqueezing transform and improved two-dimensional convolutional neural network," *Meas. Sci. Technol.*, vol. 33, no. 8, Aug. 2022, Art. no. 085002.

[25] W. Huang, J. Cheng, Y. Yang, and G. Guo, "An improved deep convolutional neural network with multi-scale information for bearing fault diagnosis," *Neurocomputing*, vol. 359, pp. 77–92, Sep. 2019.

[26] W. Fuan, J. Hongkai, S. Haidong, D. Wenjing, and W. Shuaipeng, "An adaptive deep convolutional neural network for rolling bearing fault diagnosis," *Meas. Sci. Technol.*, vol. 28, no. 9, Sep. 2017, Art. no. 095005.

[27] M. Skowron, M. Wolkiewicz, and G. Tarchala, "Stator winding fault diagnosis of induction motor operating under the field-oriented control with convolutional neural networks," *Bull. Polish Acad. Sci.*, vol. 68, no. 5, pp. 1039–1048, Oct. 2020.

[28] S. Ray, B. Ganguly, and D. Dey, "Identification and classification of stator inter-turn faults in induction motor using wavelet kernel based convolutional neural network," *Electr. Power Compon. Syst.*, vol. 48, nos. 12–13, pp. 1421–1432, Aug. 2020.

[29] M. Skowron, T. Orlowska-Kowalska, M. Wolkiewicz, and C. T. Kowalski, "Convolutional neural network-based stator current data-driven incipient stator fault diagnosis of inverter-fed induction motor," *Energies*, vol. 13, no. 6, p. 1475, Mar. 2020.

[30] D. R. Sawitri, M. A. Heryanto, H. Suprijono, M. H. Pumomo, and B. Kusumoputro, "Vibration-signature-based inter-turn short circuit identification in a three-phase induction motor using multiple hidden layer back propagation neural networks," *Int. Rev. Electr. Eng.*, vol. 13, no. 2, pp. 98–106, 2018.

[31] C. H. Park, H. Kim, J. Lee, G. Ahn, M. Youn, and B. D. Youn, "A feature inherited hierarchical convolutional neural network (FI-HCNN) for motor fault severity estimation using stator current signals," *Int. J. Precis. Eng. Manuf.-Green Technol.*, vol. 8, no. 4, pp. 1253–1266, Jul. 2021.
[32] P. Kumar and A. S. Hati, "Convolutional neural network with batch normalisation for fault detection in squirrel cage induction motor," *IET Electr. Power Appl.*, vol. 15, no. 1, pp. 39–50, Jan. 2021.
[33] S. Li, G. Liu, X. Tang, J. Lu, and J. Hu, "An ensemble deep convolutional neural network model with improved D-S evidence fusion for bearing fault diagnosis," *Sensors*, vol. 17, no. 8, p. 1729, Jul. 2017.
[34] Z. Wu, H. Jiang, S. Liu, and K. Zhao, "A deep ensemble dense convolutional neural network for rolling bearing fault diagnosis," *Meas. Sci. Technol.*, vol. 32, no. 10, Oct. 2021, Art. no. 104014.
[35] S. Liu, H. Jiang, Y. Wang, K. Zhu, and C. Liu, "A deep feature alignment adaptation network for rolling bearing intelligent fault diagnosis," *Adv. Eng. Informat.*, vol. 52, Apr. 2022, Art. no. 101598.
[36] H. Li, J. Huang, and S. Ji, "Bearing fault diagnosis with a feature fusion method based on an ensemble convolutional neural network and deep neural network," *Sensors*, vol. 19, no. 9, p. 2034, Apr. 2019.
[37] Y. Kaya, M. Kuncan, K. Kaplan, M. R. Minaz, and H. M. Ertunç, "A new feature extraction approach based on one dimensional gray level co-occurrence matrices for bearing fault classification," *J. Exp. Theor. Artif. Intell.*, vol. 33, no. 1, pp. 161–178, Jan. 2021.
[38] M. Kuncan, "An intelligent approach for bearing fault diagnosis: Combination of 1D-LBP and GRA," *IEEE Access*, vol. 8, pp. 137517–137529, 2020.
[39] H. Zhao, X. Yang, B. Chen, H. Chen, and W. Deng, "Bearing fault diagnosis using transfer learning and optimized deep belief network," *Meas. Sci. Technol.*, vol. 33, no. 6, Mar. 2022, Art. no. 065009.
[40] H. Yang, X. Li, and W. Zhang, "Interpretability of deep convolutional neural networks on rolling bearing fault diagnosis," *Meas. Sci. Technol.*, vol. 33, no. 5, Feb. 2022, Art. no. 055005.
[41] S. Bayram, K. Kaplan, M. Kuncan, and H. M. Ertunç, "The effect of bearings faults to coefficients obtaned by using wavelet transform," in *Proc. 22nd Signal Process. Commun. Appl. Conf. (SIU)*, Trabzon, Turkey, Apr. 2014, pp. 991–994.
[42] J.-M. Lee, C. Yoo, S. W. Choi, P. A. Vanrolleghem, and I.-B. Lee, "Nonlinear process monitoring using kernel principal component analysis," *Chem. Eng. Sci.*, vol. 59, no. 1, pp. 223–234, Jan. 2004.
[43] M. J. Er, S. Wu, J. Lu, and H. L. Toh, "Face recognition with radial basis function (RBF) neural networks," *IEEE Trans. Neural Netw.*, vol. 13, no. 3, pp. 697–710, May 2002.

XIAO SONG received the B.S. degree in electrical engineering and automation and the M.E. degree in power system and automation from Guangxi University, Nanning, China, in 2006 and 2009, respectively. He is currently pursuing the Ph.D. degree in safety science and engineering with the School of Safety Science and Engineering, Anhui University of Science and Technology (AUST), Huainan, China. His current research interests include electric equipment fault diagnosis, the online monitoring of motor and cable status, and intelligent algorithm.

YELIN HU was born in 1962. He received the Ph.D. degree in physics from the China University of Mining and Technology, Xuzhou, China, in 2010. He has been with the Anhui University of Science and Technology, Huainan, China, since 1990, where he is currently a Professor with the School of Electrical and Information Engineering. His current research interests include automatic control engineering and the fault diagnosis of electrical machines.

BIN DAI received the B.S. degree in electrical engineering and automation from Henan Polytechnic University, Jiaozuo, China, in 2015, and the M.S. degree in electrical engineering from the Anhui University of Science and Technology (AUST), Huainan, China, in 2022. He is currently a Lecturer with the School of Electrical and Information Engineering, AUST. His research interests include system simulation and fault diagnosis.

XIAOLIANG ZHENG received the Ph.D. degree in safety engineering from the Anhui University of Science and Technology (AUST), Huainan, China, in 2018. He is currently a Professor with the School of Electrical and Information Engineering, AUST. His current research interests include mining electromechanical system monitoring and coal mine safety monitoring and control.